

RESEARCH ARTICLE

Multicolored structural coloration of carbon nanotube fibers

Run Li | Shiliang Zhang | Hang Chen | Ya Huang | Baoshun Wang |
 Xueke Wu | Qinyuan Jiang | Siming Zhao | Fei Wang | Yanlong Zhao |
 Rufan Zhang 

Beijing Key Laboratory of Green Chemical Reaction Engineering and Technology, Department of Chemical Engineering, Tsinghua University, Beijing, China

Correspondence

Rufan Zhang, Beijing Key Laboratory of Green Chemical Reaction Engineering and Technology, Department of Chemical Engineering, Tsinghua University, Beijing 100084, China.

Email: zhangrufan@tsinghua.edu.cn

Funding information

National Natural Science Foundation of China, Grant/Award Numbers: 22075163, 51872156; National Key Research Program, Grant/Award Numbers: 2020YFC2201103, 2020YFA0210702

Abstract

Carbon nanotube fibers (CNTFs) are endowed with excellent mechanical, electrical, and thermal properties and are considered promising candidates in numerous cutting-edge fields. However, the inherent black color of CNTFs hinders their practical application in fields with high aesthetic requirements such as wearable devices and smart textiles. Due to the smooth surface and chemical inertness, CNTFs are hard to be dyed by conventional chemical dyes or colorful inks. Herein, we realize a structural coloration of CNTFs by coating them with two metal oxide layers via atomic layer deposition. The three elements of color, that is, hue, saturation, and brightness, can be controlled by adjusting the types and thickness of each oxide layer. Colorful CNTFs with wide color gamut and high saturation are achieved through different combinations. A film interference model is also established to reveal the mechanism of the structural coloration, which is a comprehensive result of thin-film interference and surface roughness briefly. The calculated reflectance well fits the measured results by introducing surface roughness parameters. Moreover, the colored CNTFs are not iridescent because of retinal signal delay, which will further expand their applications.

KEYWORDS

atomic layer deposition, carbon nanotube, structural color

1 | INTRODUCTION

Carbon nanotubes (CNTs) have attracted worldwide attention because of their extraordinary mechanical,¹ electrical,^{2,3} and thermal performance⁴ as well as other unique properties.^{5,6} CNTs are also known as ultra-black material due to their high absorbance (>90%) and chem-

ically inert surfaces, which make them almost impossible to be dyed by conventional chemical dyes and pigments.⁷ The dull and tedious black color of CNTs restricts their applications in many areas such as smart textiles, wearable devices, and functional coatings.^{8–10} In the previous studies, CNTs with narrow chirality distribution exhibit certain colors, while they are limited to single-walled CNTs with a high chirality concentration.^{11–13} The synthesis of colorful CNTs based on chirality and atomic structures is

Run Li and Shiliang Zhang contributed equally to this study.

This is an open access article under the terms of the [Creative Commons Attribution](https://creativecommons.org/licenses/by/4.0/) License, which permits use, distribution and reproduction in any medium, provided the original work is properly cited.

© 2023 The Authors. *SusMat* published by Sichuan University and John Wiley & Sons Australia, Ltd.

highly demanding and cannot meet the requirement of practical applications.¹⁴ Moreover, Peng et al. synthesized CNT/polydiacetylene nanocomposite fibers that respond to electrical current with certain color change,¹⁵ and they further reported a color-tunable, weavable fiber-shaped polymer light-emitting electrochemical cell with special and complicated design.¹⁶ However, the progress did not solve the coloration of pure CNT fibers (CNTFs). It has been a long-lasting challenge to realize the coloration of CNTs regardless of their chiral structures.

According to the coloration mechanism, colors in nature can be divided into two categories: pigment and structural colors.^{17–19} Inspired by colors in nature, structural coloration is a possible way to color CNTs. Based on the principle of physical optics, structural color processes materials into periodic structures on micro or nano scales.^{20–23} Due to the resonance characteristics of micro/nanostructures, their resonant wavelengths are affected by the size and period of the structure.²⁴ Under the illumination of white light, light of specific color can be scattered on the surface of materials.²⁵ However, compared with two-dimensional surfaces, the structural coloration of fibers with three-dimensional high curvature surfaces is usually incompatible with mainstream technologies.²⁶ Especially, different from conventional polymer fibers, CNTFs have rough and uneven surfaces, which makes it much more difficult constructing micro/nanostructures on them. Recently, we realized a structural coloration of CNTFs by coating them with thin layers of amorphous (TiO_2) via atomic layer deposition (ALD).²⁷ However, the color range was narrow, and only a few types of colors were exhibited. Moreover, the structural color usually looks very dim and even disappears when the TiO_2 layer is thicker than 300 nm, which seriously weakens the performance of colorful CNTFs.

In this work, we realized a bright and brilliant structural coloration of CNTFs by coating them with bilayer metal oxide films. Oxides including alumina (Al_2O_3), zinc oxide (ZnO), and TiO_2 can be deposited and combined freely, achieving colors with different hue, saturation, and brightness. By adjusting the combination and thickness of each layer, almost all colors with controllable brightness and saturation were obtained. Besides, the obtained structural colors of CNTFs were noniridescent that avoided the confusing color dependence on the viewing angles. The coatings tightly combined with CNTFs, and it was confirmed that the intrinsic excellent properties of CNTFs were not affected.²⁷ Moreover, the interference mechanism of bilayer film on CNTFs was investigated and corrected by introducing interface coarseness and undulation. The corrected model was close to the actual situation, and the calculated results by the corrected model were in good agreement with the experimental results. The bilayer oxide film-assisted structural coloration of CNTFs can be real-

ized in a large and controllable color gamut, which will facilitate the practical applications of CNTFs in fields of intelligent sensors, displays, functional coatings, stealth, or other color-related areas.

2 | RESULTS AND DISCUSSION

The schematic illustration of the fabrication process of bilayer film-coated CNTFs is shown in Figure 1A. The oxide layers were deposited onto CNTFs via ALD. Organic metal precursors and water vapor were introduced to the reaction chamber alternately in each cycle. Under a suitable temperature (150°C in this work), organic metal precursors reacted with water and formed corresponding metal oxide. The thickness of metal oxide layer was controlled by adjusting the ALD cycle numbers (one cycle corresponds to 0.1 nm in thickness approximately).^{27,28} The morphology changes of CNTFs before and after the ALD process are shown in Figures 1B–E and S1 in the Supplementary Information. The pristine CNTFs had rough surfaces, and the gullies formed during fiber twisting were clearly exhibited (Figures 1C and S1A,B). It can be seen from Figure 1D that pristine CNTFs were composed of CNT bundles with certain orientations and various sizes. After the ALD process, the surface became much smoother and flatter with fewer gullies (Figures 1D,E and S1C,D). Besides, as shown in the inset of Figure 1E, there were also nanoscale wrinkles on the surface of the oxide layers, but the sizes of CNT bundles were larger after deposition because of the oxide coating. To confirm the successful deposition of bilayer films, the same ALD process using TiO_2 and ZnO as an example of bilayer film was also conducted on a flat silicon wafer. The scanning electron microscopy (SEM) image (Figure 1F) and energy X-ray dispersive spectroscopy element mapping results (Figure 1G–I) showed that the bottom TiO_2 layer and the upper ZnO layer were deposited on the surface of the silicon wafer, verifying the successful construction of bilayer film.

The dense oxide layers on the surfaces play a key role in the appearance of structural color (Figure S2). By analyzing the elements and their contents on the surfaces of a bilayer film-coated CNTF with TiO_2 at the bottom and ZnO at the top of the film, only Zn and O were detected, which proved that the bilayer film was well distributed and compact in the ALD process (Figure 2A–C). Moreover, the Zn and O element content ratio was around 4:1, which also confirmed that the top layer film was mainly composed of ZnO (Figure 2D) instead of other valence compounds. A transmission electron microscopy (TEM) image (Figure 2E) clearly showed the morphology of oxide films-coated CNT bundles. In accordance with our

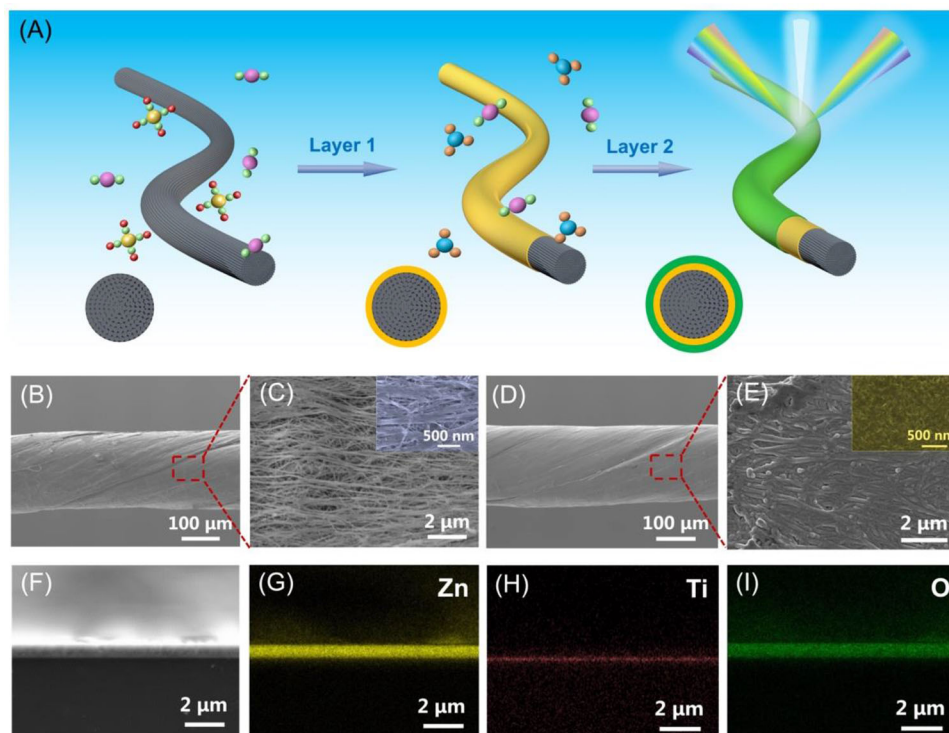


FIGURE 1 Fabrication and structural characterization of colored Carbon nanotube fibers (CNTFs). (A) Schematic illustration of the fabrication process of bilayer film-coated CNTFs. The oxides are ZnO, TiO₂, and Al₂O₃ in this work. (B–D) scanning electron microscopy (SEM) images of the pristine CNTF (B, C) and bilayer film-coated CNTF (D, E). (F–I) SEM image (F) and corresponding EDS elemental mapping images (G–I) of the cross-section of bilayer film-coated silicon wafer showing the successful deposition of the two oxide layers (TiO₂ and ZnO).

previous results,²⁷ both the TiO₂ and Al₂O₃ exhibited an amorphous phase (Figure 2G), while the ZnO exhibited a crystalline phase (Figure 2F,G). This is because the hexagonal phase of ZnO is very stable in ambient conditions, and the ZnO films produced through ALD are all hexagonal phase.^{29,30} In addition, it has been reported that strong (110) reflections would arise from films with thickness in the range of hundreds to thousands of nanometers, especially at low growth temperature,^{31–33} which is consistent with our results (Figure 2F,G). As illustrated in Figure 2F, the (110) plane of ZnO is clearly exhibited. The hexagonal phase of ZnO was further confirmed by X-ray diffraction (XRD) (Powder Diffraction File (PDF) no. 75-0576, Joint Committee on Powder Diffraction Standards; Figure 2G). The film prepared by the ALD method not only exhibited good conformability with the substrate but also would not cause any damage to the substrate. Raman spectrum also revealed the nondestruction of ALD (Figure 2H). There were three characteristic peaks at 1350, 1580, and 2700 cm⁻¹ before and after deposition, corresponding to the D-band, G-band, and 2D-band, respectively. The ratio of D-band to G-band (I_G/I_D) did not increase, confirming that the ALD method was nondestructive to CNTFs.

X-ray photoelectron spectroscopy (XPS) was carried out to reveal the valence states of the bilayer film-coated CNTFs (Figures 2I–L and S3). For a TiO₂&ZnO-coated CNTF (TiO₂ as the bottom layer and ZnO as the upper layer, the same case for other similar expressions), Zn element was clearly observed (Figure 2I). There are four deconvoluted C1s peaks at 248.78 eV, 532.85 eV, 285.93 eV, and 290.28 eV, attributed to C–C, C–O–C, C=O, and O=C–Ti bonding (Figure 2J,K), respectively. The existence of O=C–Ti bonding proved that the oxide film was coated on CNTFs tightly with certain chemical binding force rather than just mechanical bond, so the film played an important role in protecting CNTFs besides coloration. The high-resolution Zn 2p XPS spectra show a pair of peaks (Zn 2p_{3/2} and Zn 2p_{1/2}) at 1022.5 and 1045.7 eV respectively, which could be ascribed to ZnO configuration.

As shown in Figures 3 and S4, the bilayer film-coated CNTFs exhibited bright and brilliant colors. By changing the combination and thickness of different oxides, almost all types of colors with controllable brightness and saturation could be obtained (Figure 5B, will be discussed later). It was roughly divided into four color systems, that is, purple, blue, green, and yellow (corresponding to the first line to the fourth line in Figure 3)

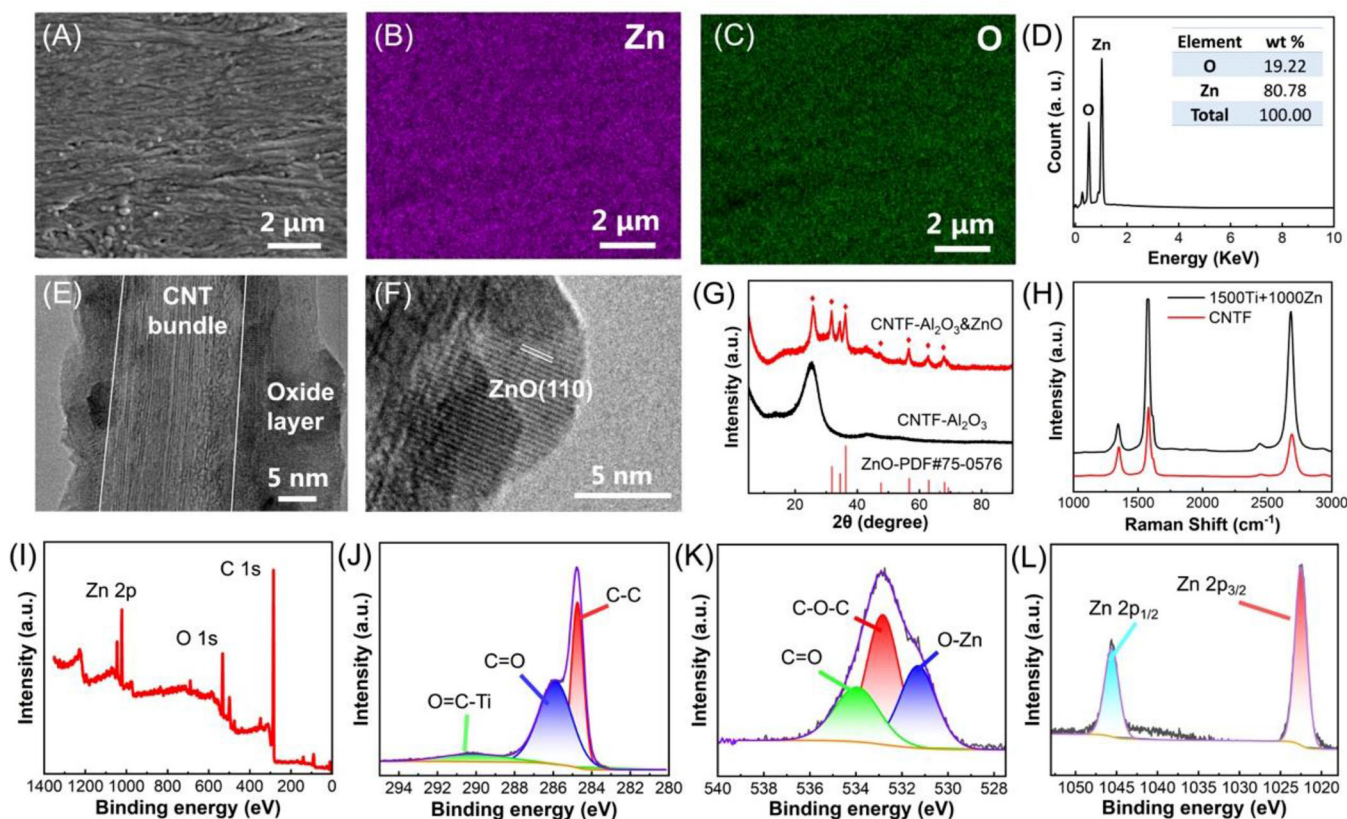


FIGURE 2 Characterization of bilayer film-coated CNTFs. (A–D) SEM image (A), corresponding energy X-ray dispersive spectroscopy (EDS) elemental mapping images (B, C) and EDS spectrum and element mass content (D) of the surface of TiO_2 & ZnO -coated CNTFs. (E, F) transmission electron microscopy (TEM) images of bilayer film-coated CNT bundles showing the ZnO crystal. (G) XRD patterns of Al_2O_3 and Al_2O_3 & ZnO -coated CNTFs. (H) Raman spectrum of a pristine and TiO_2 & ZnO -coated CNTF. (I) X-ray photoelectron spectroscopy (XPS) spectrum of a TiO_2 & ZnO -coated CNTF. (J–L) XPS spectra of C 1s, O 1s, and Zn 2p for a TiO_2 & ZnO -coated CNTF.

according to the wavelengths (corresponding to the color bar in the left in Figure 3). Moreover, independent red and silver colors and transitional cyan and chartreuse colors were also put at the bottom line in Figure 3. The typical photos of structural-colored CNTFs are shown in Figure S4. The samples exhibited were mainly TiO_2 & ZnO and Al_2O_3 & TiO_2 bilayer combinations, and the colors obtained are shown in Figures 3 and 5B. It can also be seen that CNTFs coated with 500 ALD cycles ZnO and 500 ALD cycles Al_2O_3 exhibited red color. Therefore, it is reasonable to estimate that all the colors can be obtained by regulating film thickness, combinations, and orders.

The colors exhibited a kind of regularity with the corresponding film combination and thickness. A general rule in Figure 3 is that with the increase in total thickness, the saturation and brightness first showed a trend of increase and then decrease after reaching a peak. To further investigate the relationship between the properties of bilayer films and colors, the reflectance of all the TiO_2 & ZnO and Al_2O_3 & TiO_2 -coated samples were measured (Figure S5,S6). Figure 4A,B,E,F are the reflectance results classified by color categories that have four dif-

ferent categories, that is yellow, green, purple, and blue. Although the curves look confusing at first sight, there are still some regularities. As is known, color can be described by three elements, hue, saturation, and brightness. With the increase of film thickness, the difference between peak and valley indicating the saturation of color showed a tendency of first increasing and then decreasing, and the number of peaks increased, indicating that the light paths were more complex with the increase of film thickness. When the total layer thickness of the bilayer film was as thick as 400 nm (such as the 2000Ti+2000 Zn sample shown in Figure 4E), there were many reflection peaks and the color of CNTFs was pretty dark (Figure S7). Therefore, the thickness of each layer was limited to 200 nm in this work. To better understand the relationship between the bilayer films and the structural colors, two cases were specifically discussed. First, for the Al_2O_3 & TiO_2 combination, the bottom TiO_2 film was fixed as 1500 ALD cycles (150 nm approximately²⁷) and the ALD cycles of the top layer were changed from 500 to 2000 cycles with a step size of 500 cycles (Figure 4D). As shown in Figure 4C, the reflection peak showed a red shift and the average



FIGURE 3 Optical images of colored bilayer film-coated CNTFs. Purple, blue, green, and red CNTFs were exhibited from the first line to the fourth line. Red, silver, cyan, and chartreuse CNTFs were exhibited at the bottom line. 1000Al+1000Ti representing the bottom layer is Al_2O_3 deposited for 1000 cycles and the top layer is TiO_2 deposited for 1000 cycles (it is the same case for other similar expressions).

reflectance increased with the top layer thicker, and the color of CNTFs turned from blue to green (inset optical images in Figure 4C). In addition, for the TiO_2 & ZnO combination, by fixing the total cycle number as 2500 cycles and changing the thickness of each layer (Figure 4H), the reflection peak showed a red shift with the top layer becoming thinner and the bottom layer becoming thicker, and the difference between reflection peak and valley is larger (Figure 4G), indicating that the colors had higher saturation (inset images in Figure 4G).

Based on the above analysis, we then investigated the mechanism for the generation of structural colors of bilayer film-coated CNTFs. The situation of bilayer film was much more complicated than a single film. Taking a TiO_2 & Al_2O_3 -coated CNTF as an example, as illustrated in Figures 5A and S8, there are four substances (the

CNTF, bottom oxide [Oxide 1], top oxide [Oxide 2] and air) and three interfaces composed by adjacent substrates. The mechanism of the structural coloration of CNTFs was believed to be film interference, and the light paths are shown in Figure 5A. Briefly speaking, film interference is attributed to different refractive indexes of films, which is common in life and has been widely studied. One of the most common phenomena is colorful soap bubbles under the sun. The light wave will be partially reflected by the upper and lower interfaces of the film, and new light waves will be formed due to interference. Due to the different film thicknesses and viewing angles, different colors are reflected from the internal and external surfaces, which makes them look colorful. The principle is similar for the bilayer film-coated CNTFs. When adding a new layer to the original film, the light paths were more complex, thus

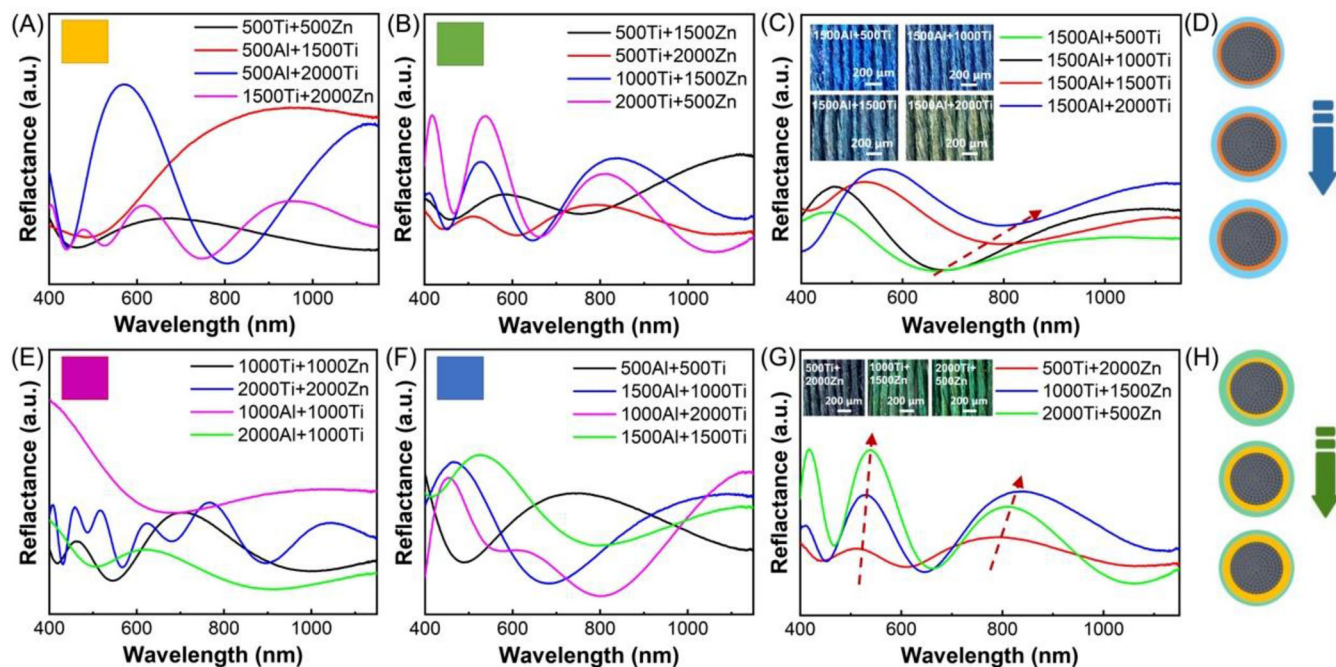


FIGURE 4 Reflectance curves of bilayer film-coated CNTFs. (A, B, E, F) Reflectance curves of yellow (A), green (B), purple (E), and blue (F) CNTFs. (C, D) Reflectance curves (C) and schematic illustration (D) of fixed bottom layer thickness samples. (G, H) Reflectance curves (G) and schematic illustration (H) of fixed total layer thickness samples.

resulting in more attractive colors (Figures 5B and S14), compared with single-layer film interference.²⁷

A model to explain the mechanism was also established. Wave optics module in COMSOL Multiphysics 5.6 is a powerful tool to simulate the optical properties of colored CNTFs. First, the fiber surface was divided into several micro-regions, and each region could be seen as a plane surface coated with two different oxide films when its size was small enough, compared to the size of CNTFs, suggesting that the structural colors of colorful CNTFs were generated by the thin-film interference. The curved surfaces of CNTFs were disassembled into basic units with a size of 30*30 μm (Figure S8), and the surface could be regarded as a plane in each unit so that the complex curved surface model was decomposed and simplified to a plane surface interference model. Such a model exhibited negligible structural variation in the plane, and the refractive indices of amorphous TiO_2 and Al_2O_3 could be found in the library of COMSOL Multiphysics 5.6. However, the calculated reflectance results of this model were quite different from the measured value (flat and measured reflectance curves in Figure 5D), suggesting that it was unreasonable to take the interface as a plane. In fact, counting the size distribution of coated CNT bundles (Figures 5C and S9), the sizes of folds and bulges were concentrated around 400~600 nm, which were not negligible, compared to visible wavelength so that the roughness of CNTFs is an important factor that has to be considered. To

construct rough interfaces, three common random curves corresponding to three interfaces were generated using the following expression:

$$f(x) = H * \sum_{m=-N}^N \text{if} \left((m! = 0), \left((m^2)^{-R/2} \right) * g_1(m) * \cos(2\pi mx + u_1(m)), 0 \right),$$

where g_1 and u_1 are 1D random functions.

In fact, interface roughness included two aspects, the undulation and coarseness. The undulation can be described by the average height of the interface. A real interface was comprehensive and should take both the above two factors into consideration. Here, three parameters H , N , and R were defined as roughness parameters regulating the rough undulating surfaces together. H represents the average height of the interface. The larger the value of H is, the more undulating the interface is. N , the spatial frequency resolution, and R , the spectral exponent, represent the roughness of the interface. The larger the N and the smaller the R is, the coarser the interface is. Figure S10 shows some typical situations. It is worth mentioning that the three parameters in each function were independent so that the free degree of the whole system was nine, which was much more complex than the single-layer film system. Taking the 1000Ti+500 Zn sample as an example, the calculated results are shown in Figure 5D. It can be seen that the real interface was neither too undulating nor

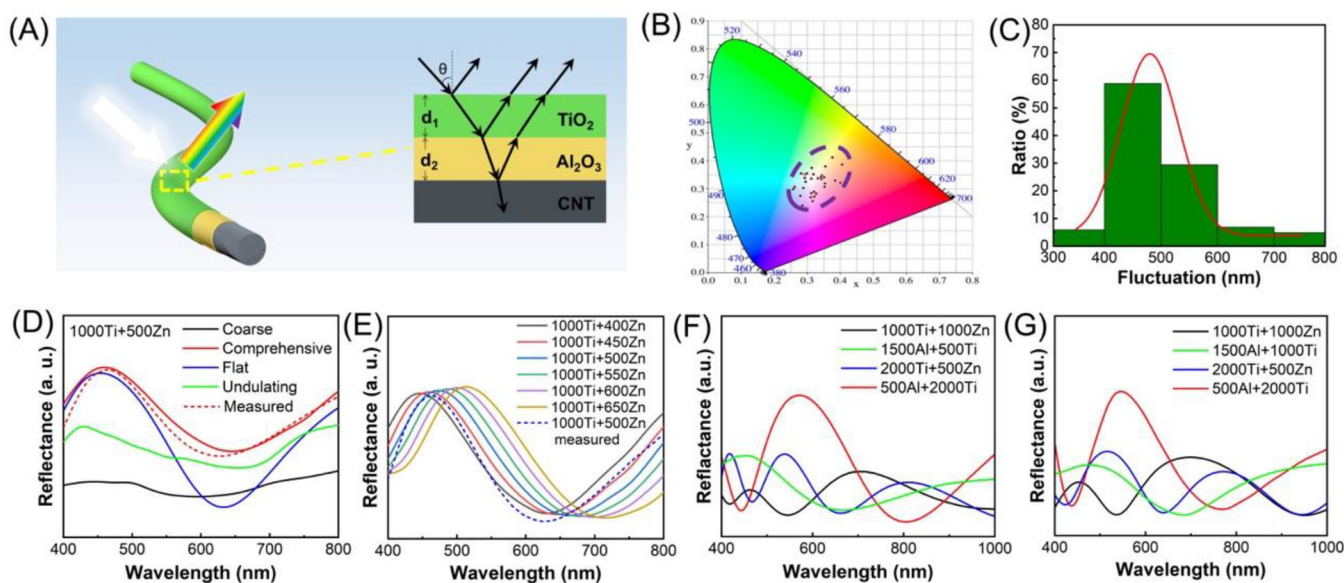


FIGURE 5 Schematic illustration and reflectance measurement and calculation of colored CNTFs. (A) Schematic illustration of thin-film interference on the surface of a bilayer film-coated CNTF. (B) Commission Internationale de l'Eclairage Chromaticity diagram (CIE) color coordinates of prepared colored CNTFs. (C) Size distribution and the fitted curve of coated CNT bundles. (D) Reflectance results of bilayer film-coated CNTFs of different surface roughness. (E) Reflectance curves of bilayer film-coated CNTFs with fixed bottom layer thickness and varied top layer thickness. (F, G) Measured (F) and calculated (G) reflectance curves of some typical samples.

too coarse, and only by comprehensively considering the two factors can a reasonable result be obtained. In addition, although the deposition thickness of ALD per cycle was about 0.1 nm, the thickness after several thousand cycles of deposition was not so determined due to the error accumulation effect. Figure 5E gives the calculation results of different top-layer thicknesses in 5 nm (50 ALD cycles) steps. It can be seen that when the top-layer thickness was changing in a small range, the calculated reflectance was similar. Results were similar when the top layer was fixed and only the bottom layer was changed (Figure S11A). In fact, the closest calculation result to the measured reflectance of sample 1000Ti+500 Zn was 1000Ti+450 Zn instead of 1000Ti+500 Zn. However, when the thickness changed greatly (i.e., 50 nm), there were obviously different reflectance curves as shown in Figure S11B. Therefore, thickness was also an important variable to be considered in the model, which made the free degree of the whole system higher. After the above correction, as shown in Figure 5F,G, the calculated reflectance agreed with the measured reflectance well, suggesting the modified rough surface interference model was applicable.

Another important feature of the bilayer film-coated CNTFs is the noniridescence of the structural colors. For conventional film interference, when the film is uniform, interference fringes of different colors will be formed due to the different reflected light paths inside and outside the film at different view angles. Therefore, the film interference fringes caught by the eyes should be iridescent

and angle-dependent. However, different from rainbow or soap bubbles, the rough and irregular surfaces of bilayer film-coated CNTFs caused the incident angle that was not constant at different positions, which resulted in the non-iridescent and angular independent color. When light with different frequencies reaches the human retina, the electrical signals generated by two different frequencies or composite light with a tiny time interval will have a superposition effect. That is to say, the electrical signal generated by the previous optical signal has not been completed, while the latter optical signal has arrived, so the signal superposition is generated. Therefore, the electrical signal was generated by neither the former optical signal nor the latter optical signal but a composite result of the two optical signals. Compared with the iridescent structural color, the colors of bilayer film-coated CNTFs avoid the confusing colors depending on view angles.³⁴

3 | CONCLUSION

In conclusion, multicolored CNTFs were successfully fabricated by depositing two layers of different metal oxides via ALD. Almost all colors can be obtained by combining different oxides and adjusting the thickness of each layer. The structural coloration of CNTFs is a comprehensive result of thin-film interference and surface roughness. Roughness parameters are introduced in our model using the wave optics module in COMSOL Multiphysics 5.6 to

simulate the real situation to the greatest extent. After optimization, the calculated reflectance is in good agreement with the actual results. Moreover, the prepared CNTFs are not iridescent due to the rough surface of CNTFs, avoiding confusing colors depending on view angles, which is very practical in various applications.

4 | EXPERIMENTAL SECTIONS

4.1 | Materials

CNTFs were obtained from Tanrand Technology. Titanium (IV) isopropoxide (TIP; 99.999% metals basis) was purchased from Aladdin Industrial Co., Ltd., Trimethyl aluminum (TMA; 1.0 M in hexane) was purchased from J&K Scientific. Diethyl zinc (DEZ; 1.0 M in hexane) was purchased from Meryer Biochemical Technology Co., Ltd. Deionized water was from a Milli-Q Plus 185 ultra-pure water purification system with a resistivity of 18.2 megohm·cm. Absolute ethanol ($\text{CH}_3\text{CH}_2\text{OH}$, analytical grade) was provided by Sinopharm chemical reagent Co., Ltd.

4.2 | Fabrication of structural colored CNTFs

The metallic oxide was introduced to CNTFs by ALD. A complete ALD cycle involves six steps, which are pulse, exposure, and purge of organometallic precursors and water. The duration of each step is different for different precursors. Specifically, the pulse, exposure and purge time for TIP are 0.4, 8, and 25 s; 0.02, 8, and 25 s for DEZ; 0.02, 8, and 25 s for TMA; 0.1, 8, 30 s for water (H_2O) respectively. Precursors were introduced to the reaction chamber by nitrogen (N_2) as carrier gas. In particular, TIP needs to be preheated to 80°C , while others at room temperature. The reaction was in a vacuum chamber at 150°C . To construct bilayer film-coated CNTFs, two different oxides were deposited successively. The film thickness of each layer was controlled by depositing cycles, and the whole reaction usually lasted for dozens of hours.

4.3 | Characterization

SEM images were obtained using a JSM7401F (JEOL Ltd.) electron microscope with an accelerating voltage of 5.0 kV and a beam current of $20\ \mu\text{A}$. TEM images were taken using a JEM-2010 (JEOL Ltd.) transmission electron microscope

with an accelerating voltage of 120 kV. The chemical valence state of the atoms was investigated by XPS (SPM-9700, SHIMADZU Co.) with an $\text{Al-K}\alpha$ radiation source (1486.6 eV) under an ultrahigh vacuum (1×10^{-9} mbar). The phase composition and crystalline structure were revealed by an XRD spectrometer (Bruker D8 Advance Diffractometer) equipped with a $\text{Cu-K}\alpha$ radiation source at the scanning rate of $5^\circ/\text{min}$ in the 2θ range from 5° to 90° . Raman spectra were collected at ambient conditions with a Horiba HR 800 spectrometer equipped with an excitation laser of 532 nm. Optical images of samples were taken using a digital camera (Nikon DSLR D5100) and an optical microscope (Olympus BX53m) under ordinary white light. Reflectance curves were recorded using a PG2000-Pro spectrometer (Idea Optics Co. Ltd., China).

AUTHOR CONTRIBUTIONS

Rufan Zhang, Run Li, and Shiliang Zhang conceived the project and designed the experiments. Run Li, Shiliang Zhang, and Hang Chen conducted the experiments. Run Li wrote the paper. Ya Huang, Baoshun Wang, Xueke Wu, Qinyuan Jiang, Siming Zhao, Fei Wang, and Yanlong Zhao participated in the discussion and analysis of experimental results. Rufan Zhang supervised the project. All authors discussed the results and commented on the manuscript.

ACKNOWLEDGMENTS

This work is supported by National Natural Science Foundation of China (Grant Nos. 22075163 and 51872156) and National Key Research Program (2020YFC2201103, 2020YFA0210702).

CONFLICT OF INTEREST

The authors declare no conflict of interest.

ORCID

Rufan Zhang  <https://orcid.org/0000-0003-1774-0550>

REFERENCES

1. Bai Y, Zhang R, Ye X, et al. Carbon nanotube bundles with tensile strength over 80 GPa. *Nat Nanotechnol*. 2018;13(7):589-595.
2. Dai H, Wong EW, Lieber CM. Probing electrical transport in nanomaterials: conductivity of individual carbon nanotubes. *Science*. 1996;272(5261):523-526.
3. Javey A, Guo J, Wang Q, et al. Ballistic carbon nanotube field-effect transistors. *Nature*. 2003;424(6949):654-657.
4. Zhang R, Zhang Y, Wei F. Horizontally aligned carbon nanotube arrays: growth mechanism, controlled synthesis, characterization, properties and applications. *Chem Soc Rev*. 2017;46(12):3661-3715.
5. Li R, Jiang Q, Zhang R. Progress and perspective on high-strength and multifunctional carbon nanotube fibers. *Science Bulletin*. 2022;67(8):784-787.

6. Bai Y, Yue H, Wang J, et al. Super-durable ultralong carbon nanotubes. *Science*. 2020;369(6507):1104-1106.
7. Yang Z-P, Ci L, Bur JA, et al. Experimental observation of an extremely dark material made by a low-density nanotube array. *Nano Lett*. 2008;8(2):446-451.
8. Shi X, Zuo Y, Zhai P, et al. Large-area display textiles integrated with functional systems. *Nature*. 2021;591(7849):240-245.
9. Janas D, Cabrero-Vilatela A, Bulmer J, et al. Carbon nanotube wires for high-temperature performance. *Carbon*. 2013;64:305-314.
10. Janas D, Koziol KK. Rapid electrothermal response of high-temperature carbon nanotube film heaters. *Carbon*. 2013;59:457-463.
11. Green AA, Hersam MC. Colored semitransparent conductive coatings consisting of monodisperse metallic single-walled carbon nanotubes. *Nano Lett*. 2008;8(5):1417-1422.
12. Liao Y, Jiang H, Wei N, et al. Direct synthesis of colorful single-walled carbon nanotube thin films. *J Am Chem Soc*. 2018;140(31):9797-9800.
13. Yanagi K, Miyata Y, Tanaka T, et al. Colors of carbon nanotubes. *Diam Relat Mater*. 2009;18(5-8):935-939.
14. Wei N, Tian Y, Liao Y, et al. Colors of single-wall carbon nanotubes. *Adv Mater*. 2021;33(8):2006395.
15. Peng H, Sun X, Cai F, et al. Electrochromatic carbon nanotube/polydiacetylene nanocomposite fibres. *Nat Nanotechnol*. 2009;4(11):738-741.
16. Zhang Z, Guo K, Li Y, et al. A colour-tunable, weavable fibre-shaped polymer light-emitting electrochemical cell. *Nat Photon*. 2015;9(4):233-238.
17. Srinivasarao M. Nano-optics in the biological world: beetles, butterflies, birds, and moths. *Chem Rev*. 1999;99(7):1935-1961.
18. Yuan W, Li Q, Zhou N, et al. Structural color fibers directly drawn from colloidal suspensions with controllable optical properties. *ACS Appl Mater Inter*. 2019;11(21):19388-19396.
19. Xuan Z, Li J, Liu Q, et al. Artificial structural colors and applications. *Innovation*. 2021;2(1):100081.
20. Zhao Y, Xie Z, Gu H, et al. Bio-inspired variable structural color materials. *Chem Soc Rev*. 2012;41(8):3297-3317.
21. Sun S, Zhou Z, Zhang C, et al. All-dielectric full-color printing with TiO₂ metasurfaces. *ACS Nano*. 2017;11(5):4445-4452.
22. Ko SH. Materials science crazy colour. *Nature*. 2019;570(7761):312-313.
23. Gawlik BM, Cossio G, Kwon H, et al. Structural coloration with hourglass-shaped vertical silicon nanopillar arrays. *Opt Exp*. 2018;26(23):30952-30968.
24. Won D, Ko SH. The colour of stress. *Nat Mater*. 2022;21(9):997-998.
25. Dumanli AG, Savin T. Recent advances in the biomimicry of structural colours. *Chem Soc Rev*. 2016;45(24):6698-6724.
26. Wang L, Fu X, He J, et al. Application challenges in fiber and textile electronics. *Adv Mater*. 2020;32(5):1901971.
27. Chen F, Huang Y, Li R, et al. Superdurable and fire-retardant structural coloration of carbon nanotubes. *Sci Adv*. 2022;8(26):eabn5882.
28. Brozena AH, Oldham CJ, Parsons GN. Atomic layer deposition on polymer fibers and fabrics for multifunctional and electronic textiles. *J Vac Sci Technol A*. 2016;34(1):010801.
29. Miikkulainen V, Leskela M, Ritala M, et al. Crystallinity of inorganic films grown by atomic layer deposition: overview and general trends. *J Appl Phys*. 2013;113(2):021301.
30. Lou C, Yang C, Zheng W, et al. Atomic layer deposition of ZnO on SnO₂ nanospheres for enhanced formaldehyde detection. *Sens Actuators B Chem*. 2021;329:129218.
31. Guziewicz E, Godlewski M, Krajewski T, et al. ZnO grown by atomic layer deposition: a material for transparent electronics and organic heterojunctions. *J Appl Phys*. 2009;105(12):122413.
32. Przewdziecka E, Wachnicki L, Paszkowicz W, et al. Photoluminescence, electrical and structural properties of ZnO films, grown by ALD at low temperature. *Semicond Sci Technol*. 2009;24(10):105014.
33. Wang T, Luo Z, Li C, et al. Controllable fabrication of nanostructured materials for photoelectrochemical water splitting via atomic layer deposition. *Chem Soc Rev*. 2014;43(22):7469-7484.
34. Zhang Y, Han P, Zhou H, et al. Highly brilliant noniridescent structural colors enabled by graphene nanosheets containing graphene quantum dots. *Adv Funct Mater*. 2018;28(29):1802585.

SUPPORTING INFORMATION

Additional supporting information can be found online in the Supporting Information section at the end of this article.

How to cite this article: Li R, Zhang S, Chen H, et al. Multicolored structural coloration of carbon nanotube fibers. *SusMat*. 2023;3:102-110.
<https://doi.org/10.1002/sus2.111>